Geologie en Mijnbouw **73:** 181–197, 1994.

The 1992 Roermond earthquake, the Netherlands, and its aftershocks

T. Camelbeeck[1], T. van Eck[2], R. Pelzing[3], L. Ahorner[4], J. Loohuis[2], H.W. Haak[5], P. Hoang-Trong[6] & D. Hollnack[7]

[1] *Royal Observatory Belgium, Avenue Circulaire 3, B-1180 Brussels, Belgium;* [2] *Institute of Earth Sciences, Utrecht University, P.O. Box 80 021, 3508 TA Utrecht, the Netherlands;* [3] *Geological Survey-Northrhine-Westphalen, De Greiff Str. 195, 4150 Krefeld, Germany;* [4] *Department of Earthquake Geology, Geological Institute, University of Cologne, Vinzenz Pallotti Str. 26, 51429 Bergisch Gladbach, Germany;* [5] *Section of Seismology, Royal Netherlands Meteorological Institute, P.O. Box 201, 3730 AE De Bilt, the Netherlands;* [6] *Institut de Physique du Globe, 5 Rue René Descartes, 67084 Strasbourg Cedex, France;* [7] *Lehrgebiet für Angewandte Geophysik der Rheinisch-Westfälische Technische Hochschule Aachen, Lochnerstrasse 4–20, D-5100 Aachen, Germany*

Received 15 September 1993; accepted in revised form 15 February 1994

Key words: Roer Valley Graben, seismotectonics, focal mechanisms, earthquake location

Abstract

On April 13, 1992 an $M_W = 5.4$ normal dip-slip earthquake occurred 5 km south-west of the Dutch town Roermond. It was located at a depth of 17 km near the Peel Boundary Fault in the Roer Valley Graben.

Belgian, Dutch, German and French seismologists installed 29 mobile seismograph stations for a period of two months after the main shock. Both the mobile and the permanent stations recorded more than 200 aftershocks. High-quality hypocentral locations were obtained for 55 aftershocks. Hypocenters that occurred in the vicinity of the main shock hypocenter coincide with one of the focal mechanism nodal planes, i.e. strike 127°, dip 70°. The Roermond earthquake also triggered seismic activity in the graben as far as 40 km to the southeast. Focal mechanisms were determined for 20 aftershocks. Out of the 14 with a predominantly normal fault solution, eight have a strike direction parallel, and six a strike perpendicular to the strike of the main event. A stress inversion using the 13 best constrained fault plane solutions of aftershocks located near the main shock hypocenter indicates a direction for the principal stress that is similar to that of the regional stress field.

From our experience in analyzing the data we recommend the upgrading of the existing regional recording systems to high-dynamic range seismograph stations and the installation of a number of accelerometers in the Roer Valley Graben and its surroundings.

Introduction

On April 13, 1992 at 1h20m (UT) a moderate intraplate earthquake ($M_W = 5.4$) occurred in the Lower Rhine Embayment near the Dutch city of Roermond. The earthquake was strongly felt in the border region of the Netherlands, Germany and Belgium causing damage corresponding to the intensity of VII (MSK scale) in the towns Roermond and Herkenbosch in the Netherlands and Heinsberg in Germany (Haak et al. 1994).

The Roermond earthquake occurred in the Roer Valley Graben (Geluk et al. 1994), the northwestern branch of the Rhine Graben System and part of a series of grabens extending from the Rhine Graben system in the north to the Valencia (Spain) Graben in the south (Ziegler 1992). According to Zijerveld et al. (1992) this European Cenozoic rift system started its development during the late Eocene and has been reactivated several times during its lifetime. Geological evidence for recent subsidence is presented by Zijerveld et al. (1992) and Geluk et al. (1994). Ahorner (1983) argued, using earthquake focal mechanisms and *in situ* stress measurements, that the Roer Valley Graben is presently subject to a SW–NE extension.

The Roer Valley Graben belongs together with the Belgian zone (Ahorner 1985) to the seismically most active onshore zones in northwestern Europe. According to Ambraseys (1985) at least five earthquakes with magnitude $M_S > 4.0$ occurred this century within the Roer Valley Graben and its extension. The same region has experienced four earthquakes with $M_S > 5.0$ since 1755: On December 27, 1755 and February 18, 1756 near Düren, on August 26, 1878 near Tollhausen, and on March 14, 1951 near Euskirchen, all in the German part of the Roer Valley Graben region (Ahorner et al. 1970, 1994, Ambraseys 1985, Meidow 1994).

The Roermond earthquake was followed by a large number of aftershocks recorded by both permanent and mobile seismograph stations. A rapid deployment of temporary stations by seismologists from Belgium, the Netherlands, France and Germany in the days after the earthquake resulted in a total of 29 mobile seismograph stations during a two-month period following the main shock. This network was essential in recording many of the more than 200 aftershocks.

In this paper we present the location and source parameters of the main shock, together with an initial analysis of the aftershocks, which is the result of this cooperative deployment of mobile seismograph stations.

The main shock

The main shock occurred at 01:20:02.8 UT and had its epicenter about 5 km southwest of the Dutch town of Roermond at a depth of approximately 17 km (Table 1). Its location and origin time have been determined using arrival times of 47 permanent stations in the Netherlands, Belgium, Germany and Luxembourg within a radius of 215 km distance and a simplified crustal and upper mantle velocity model with lateral homogeneous layers incorporating station corrections obtained from the aftershock analysis. The main shock was preceded by a small foreshock only a few tenths of a second before (Ahorner 1994, Oncescu et al. 1994), but otherwise no foreshock activity has been observed.

The Roermond earthquake is a pure normal dip-slip event (Table 1 and Fig. 7; see also Ahorner 1992, 1994, Dziewonski et al. 1993, Paulssen et al. 1992) and fits well the existing stress models for the region, i.e. a NW–SE direction for the maximal horizontal principal stress (Ahorner 1983, Camelbeeck & van Eck 1994, Grünthal & Stromeyer 1991).

Dynamic parameters have been obtained from the SH-wave observed at seven broad-band stations: BUG, TNS, BFO, HAM, GRC, BRN and WET (Camelbeeck & van Eck 1994). The observed ground displacement spectra were corrected for geometrical spreading, average radiation pattern and surface reflection and have been interpreted using Brune's ω-square model (Brune 1970, 1971) for obtaining seismic moment, M_0, fault surface (circular with radius r_0), and static stress drop, $\Delta\sigma$. The results have been summarized in Table 1. The deduced moment magnitude (Hanks & Kanamori 1979) is $M_W = 5.4$. Similar source parameters have been obtained from local and regional data by Ahorner (1994), Paulssen et al. (1992), Pelzing (1994), Braunmiller et al. (1994) and others (Table 1).

Permanent and mobile seismograph stations

The earthquake occurred in a region with a good coverage of permanent seismograph stations run by the observatories in De Bilt (Royal Netherlands Meteorological Institute), Uccle (Observatoire Royal de Belgique), Bensberg (University of Cologne) and Krefeld (Geological Survey of Nordrhein Westfalen). Other relevant seismograph networks in the region comprise the NARS (University of Utrecht) and stations of the German Regional Seismic Network or GRSN (Geo Research Center, Potsdam). Table 2 provides a list of permanent stations used in the analysis of aftershocks.

The event was big enough to be recorded by seismographs almost all over the world. Unfortunately, in spite of the fact that the event occurred in a region with densily spaced seismograph stations, station KRN (NL) at 33 km distance turned out to be the closest seismograph. Also, no ground acceleration measurements are available from the epicentral area, due to the lack of accelerometers in the epicentral area.

Unfortunately, few stations in the region were equipped with a dynamic range large enough to record the full waveform. The closest unclipped seismogram comes from station GSH and TGA (Ahorner 1992, Pelzing 1994) at a distance of about 58 km. A full account of the available waveform data for the main shock is given in Dost & Sleeman (1994).

The main shock occurred early in the morning 3:20 h local time. Within approximately one and a half hour the observatories of Uccle, De Bilt and Bensberg had exchanged arrival times and magnitude infor-

Table 1. Source parameters of the 1992 Roermond main shock.

Authors	1	2	3	4	5	6	7
lat. (° ' N)	51 09.8	51 10.2 ± 1 km	51 10.2	51 10.1	–	–	51 33.6
long. (° ' E)	5 57.2	5 55.5 ± 1 km	5 58.2	5 55.9	–	–	5 37.8
depth (km)	17.4 ± 1	14.6 ± 3	21	17.6 ± 1	18	–	15
OT (h m s)	01 20 02.8	01 20 02.8 ± 0.1	01 20 03.1	01 20 02.4	–	–	01 20 06.7
strike (°)	127	124	124 ± 10	120 ± 10	133 ± 2	–	143
dip (°)	70	68	70 ± 10	70 ± 10	68 ± 1	–	68
rake dip (°)	- 92	- 90	- 90 ± 10	- 100 ± 10	- 100 ± 2	–	- 87
M_0 (10^{16} Nm)	14.0 ± 5.5	9.8	–	5.4	8.5 ± 0.3	11	13.3
area (km^2)	10.6 ± 4.7	15	–	5.6	–	–	–
$\bar{u}$ (cm)	33 ± 19	21	–	35	–	9–30	–
$\Delta\sigma$ (MPa)	9.7 ± 6.4	4.4	–	12	–	1–7	–
M_W	5.4 ± 0.1	5.3	–	–	5.3	5.3	5.4
M_L	5.8	5.9 ± 0.1	–	5.9	–	–	–

1. Camelbeeck & van Eck (1994) and this study; 2. Ahorner (1994); 3. Paulssen et al. (1992); 4. Pelzing (1994); 5. Braunmiller et al. (1994); 6. Grünthal & Grosser (1992); 7. Dziewonski et al. (1993).
OT – origin time; M_0 – seismic moment; $\bar{u}$ – average slip; $\Delta\sigma$ – stress drop; M_W – Moment magnitude; M_L – Local Richter magnitude.

mation and made decisions where to deploy mobile seismograph stations.

The mobile seismograph stations were installed by Belgian, Dutch, German and French seismologists with the intention to improve aftershock monitoring. The first two stations, installed by Belgian seismologists, were already operating in the epicentral region four hours after the main shock. Within one day Belgian and Dutch seismologists had installed nine mobile stations in the area around Roermond and during about two months after the main shock a total of 29 mobile seismographs have been deployed (Fig. 1, Table 3).

The types of mobile seismograph stations differed widely. The Ecole et Observatoire de Physique du Globe (EOPG) from Strasbourg installed a telemetric network consisting of eight stations. Dutch seismologists installed a three-station network with central recording in De Bilt (Lennartz MARS-88). Belgian and German seismologists installed autonomous Lennartz PCM-5800 seismographs. Two Geotech-Teledyne Portacorders were installed for quick on-site inspection of the current seismicity. All stations used the German DCF time signal for clock calibration.

The performance of the different mobile stations was satisfactory. Unfortunately, the telemetric stations of the EOPG recorded only a small fraction of the aftershocks, mainly due to logistical problems. The MARS-88 and the PCM-5800 systems of Lennartz proved to be the most valuable stations in the field.

Aftershocks

The Roermond earthquake was followed by more than 200 aftershocks. This is a large number of events compared with the regular rate of seismicity in the region. However, the number of aftershocks decreased rapidly with time (Fig. 2). Therefore, a quick deployment of mobile seismograph stations for aftershock monitoring was essential.

Aftershock occurrence

Of the more than 200 aftershocks recorded, about 100 occurred within the first 24 hours after the main shock and 50 within the first four hours (Fig. 2). A close inspection of the aftershock occurrence shows a decrease in aftershock activity eight hours after the main shock and an increased activity during the following night of April 13/14. This observation cannot be explained by a decreased detectability during daytime, as from April 13, 12 a.m. already seven mobile seismograph stations were running in the epicentral area, thus increasing our detection capabilities.

Aftershock location

Aftershock arrival time data has been gathered from the different agencies with permanent stations in the region and from agencies that employed mobile seis-

Table 2. Permanent seismograph stations used for the location of the Roermond earthquake aftershocks.

Name site	Stat. code	Lat. N°	Long. E°	Elev. m	Seismometer type	Recorder system	Agency
Grosshau (G)	GSH	50 44.34	6 22.61	– 370	WMKIIIA(3C)	Len.PCM	GLNRW(G)
Jackerath (G)	JCK	51 02.18	6 25.91	– 240	L4C-3D	Len.PCM	GLNRW(G)
Pulheim (G)	PLH	51 00.32	6 49.23	– 300	L4C-3D	Len.PCM	GLNRW(G)
Krefeld (G)	KRF	51 20.50	6 32.25	– 210	L4C-3D	Len.PCM	GLNRW(G)
Wahnbachtalsperre (G)	WBS	50 48.47	7 17.03	132	L4C-3D	Len.PCM	GLNRW(G)
Oleftalsperre (G)	OLF	50 29.73	6 25.26	473	L4C-3D	Len.PCM	GLNRW(G)
Clavier (B)	CLA	50 25.22	5 18.21	280	LE-3D	PC-ORB	ORB (B)
La Chartreuse (B)	LCH	50 38.32	5 36.08	150	L4C	PC-ORB	ORB (B)
Wortegem (B)	WOR	50 51.31	3 30.40	– 150	SM-6	PC-ORB	ORB (B)
Vianden (L)	VIA	49 56.16	6 12.22		LE-3D	Lennartz PCM	ORB(B)+L(L)
Wibrin (B)	WIB	50 09.68	5 43.54	425	L4C	Lennartz PCM	ORB (B)
Sart Tilman (B)	STI	50 35.10	5 33.84	240	L4C	PC-ORB	ORB (B)
Membach (B)	MEM	50 36.54	6 00.36	250	L4C-3D	Len. PCM	ORB (B)
Meuville (B)	MEU	50 23.87	5 46.15	335	L4C-3D	Len. PCM	ORB (B)
Robertville (B)	ROB	50 27.20	6 06.63	447	L4C-3D	Len. PCM	ORB (B)
Bougnies (B)	BOU	50 23.40	3 56.76	100	L4C	Len. PCM	ORB (B)
Seneffe (B)	SNF	50 30.52	4 17.00	125	L4C	PC-ORB	ORB (B)
Aulne (B)	AUL	50 21.96	4 20.00	120	L4C	PC-ORB	ORB (B)
Ronquieres (B)	RQR	50 36.40	4 13.56	65	L4C	PC-ORB	ORB (B)
Eben-Emael (B)	EBN	50 47.82	5 40.80	60	L4C	PC-ORB	ORB (B)
Dourbes (B)	DOU	50 05.76	4 35.64	80	L4C-3D	PC-ORB	ORB (B)
Humain (B)	HUM	50 11.60	5 15.59	293	L4C-3D	PC-ORB	ORB (B)
Lessines (B)	LES	50 42.73	3 50.68	30	L4C-3D	Len. PCM	ORB (B)
Zevekote (B)	ZEV	51 08.27	2 54.06	0	L4C	PC-ORB	ORB (B)
Uccle (B)	UCC	50 47.90	4 21.57	100	S-10	PC-ORB	ORB (B)
Walferdange (L)	WLF	49 39.88	6 09.14	200	LE-3D	Lennartz PCM	ORB(B)+L(L)
Valkenburg (NL)	VKB	50 52.01	5 47.08	90	WMKIIIA	KNMI-PCM	KNMI(NL)
Epen (NL)	ENN	50 46.03	5 55.40	120	WMKII	KNMI-PCM	KNMI(NL)
Winterswijk (NL)	WTS	51 59.73	6 48.60	43	WMKII	KNMI-PCM	KNMI(NL)
Kerkrade (NL)	KRN	50 52.50	6 04.60	– 80	WMKIIIA	KNMI-PCM	KNMI(NL)
Witteveen (NL)	WIT	52 48.80	6 40.18	17	WMKII	KNMI-PCM	KNMI(NL)
Rolde (NL)	RLD	53 00.00	6 39.51	11	WMKIIIA	KNMI-PCM	KNMI(NL)
Bovensmilde (NL)	BVS	52 59.85	6 27.57	12	WMKIIIA	KNMI-PCM	KNMI(NL)
Laaghalerveen (NL)	LGV	52 55.75	6 30.22	15	WMKIIIA	KNMI-PCM	KNMI(NL)
Marwijksoord (NL)	MWD	52 57.59	6 38.04	14	WMKIIIA	KNMI-PCM	KNMI(NL)
Westerbork (NL)	WSB	52 55.00	6 36.64	16	WMKIIIA	KNMI-PCM	KNMI(NL)
Zeyen (NL)	ZYN	53 03.18	6 32.16	10	WMKIIIA	KNMI-PCM	KNMI(NL)
Kalltalsperre (G)	KLL	50 38.80	6 18.68	390	HS10 1Hz	Len. PCM	Un.C(G)
Millendorf (G)	MIL	50 59.58	6 33.55	70	LE-3D	Len. PCM	Un.C(G)
Bergheim (G)	KIR	50 57.48	6 38.38	65	LE-3D	Len. PCM	Un.C(G)
Keuten (G)	KEN	50 56.98	6 39.44	72	LE-3D	Len. PCM	Un.C(G)
Bergheim (G)	TGB	50 57.38	6 39.26	– 250	LE-3D	Len. PCM	Un.C(G)
Bergheim (G)	TGO	50 57.38	6 39.26	50	LE-3D	Len. PCM	Un.C(G)
Bergheim (G)	TGA	50 57.55	6 39.08	50	LE-3D	Len. PCM	Un.C(G)
Bergheim (G)	TGC	50 57.25	6 39.60	50	LE-3D	Len. PCM	Un.C(G)

Continued next page.

Table 2. continued.

Name site	Stat. code	Lat. N°	Long. E°	Elev. m	Seismometer type	Recorder system	Agency
Bensberg (G)	BNS	50 57.83	7 10.54	200	LE-3D	Len. PCM	Un.C(G)
Koeppel (G)	KOE	50 25.52	7 43.90	540	S-13	Len. PCM	Un.C(G)
Burg Eltz (G)	BGG	50 12.36	7 20.23	140	S-13	Len. PCM	Un.C(G)
Julich (G)	JUE	50 54.83	6 24.59	91	LE-3D	Len. PCM	Un.C(G)
Steinbachtal (G)	STB	50 35.72	6 50.40	270	L4C	Len. PCM	Un.C(G)
Bohlendorf (G)	BOH	50 58.08	6 37.36	0	L4C	Len. PCM	Un.C(G)
Dreilagerbach (G)	DRE	50 39.79	6 13.99	394	LE-3D	MARS-88	Un.C(G)
Ochtendung (G)	OCH	50 22.25	7 22.55	120	S-13	analog	Un.C(G)
Sindorf (G)	SIN	50 55.11	6 39.95	70	LE-3D	Len. PCM	Un.C(G)
Birkenfeld (G)	RUP	49 42.10	7 03.61		S-13	Telemetry	Un.K(G)
Alteburg (G)	ABH	49 52.92	7 32.88		S-13	Telemetry	Un.K(G)
	NE40	51 58.53	6 44.10	37	SL210+SL220	NARS	Un.U(NL)
Valkenburg (NL)	NE15	50 52.02	5 47.10	100	SL210+SL220	NARS	Un.U(NL)
Krefeld (G)	NE39	51 20.85	6 32.28	40	SL210+SL220	NARS	Un.U(NL)
Bochum (G)	BUG	51 26.73	7 15.87	85	STS2	Quanterra	GRN(G)

Seismometer types and manufacturers: LE-3D – Lennartz; L4C – Mark Products; L22 – Mark Products; S-10 – Geotech- Teledyne; S-13 – Geotech-Teledyne; SL210 – Kinemetrics; SL220 – Kinemetrics; SM-6 – Sensonics; STS2 – Streckeisen; WMKII – Willmore; WMKIIIA – Willmore.
Recorder systems: Len. PCM – Lennartz Electronics system of Pulse Code Modulation (PCM); PC-ORB – Digital recording on PC developed by the ORB; KNMI-PCM – Pulse Code Modulation used at KNMI; MARS-88 – Lennartz Electronics field recording equipment; NARS – Digital recording system developed by the Inst. Earth Sciences, Un. U, NL; Quanterra – Recording system developed by Quanterra, USA.
Agencies: EOPG – Ecole et Observatoire de Physique du Globe, Strasbourg, France; GLNRW – Geologisches Landesamt Nordrhein-Westphalen, Krefeld, Germany; GRN – German Regional Network, Potsdam, Germany; KNMI – Koninklijk Nederlands Meteorologisch Instituut, De Bilt, the Netherlands; L – Musee d'Histoire Naturelle Luxembourg, Luxembourg; ORB – Observatoire Royal de Belgique, Uccle, Belgium; Un. A – Technical University of Aachen, Aachen, Germany; Un. C – University of Cologne, Bergisch Gladbach, Germany; Un. K – University of Karlsruhe, Karlsruhe, Germany; Un. U – University of Utrecht, Utrecht, the Netherlands.

mograph stations in the epicentral area (Tables 2, 3). The arrival time data is stored in a HYPO71 input file and regularly exchanged between the actively involved agencies. This procedure facilitated and improved the measuring of the arrival times. Presently, the data file contains approximately 230 probable aftershocks of which 25% have been measured by sufficient stations to enable a reliable estimation of the location.

The velocity structure of the upper crust of the Roer Valley Graben and its surroundings shows, unfortunately, large lateral variations. These velocity variations are insufficiently known to enable a hypocentral location determination using 3D velocity models. Therefore, a modified HYPO71 location program by Lienert et al. (1986) with a flat layer model and station delays to correct for local structure variations has been used. This approach is thought to be well motivated and valid for events in the direct vicinity of the main shock hypocenter.

The following master event location procedure involving the estimation of station delays has been applied. Firstly, six master events were selected. They all occurred within the epicentral area and were recorded by at least 10 stations in the graben. The location of these events were obtained using a local velocity model (NL002, Fig. 3). Model NL002 differs from other regional velocity models in that it includes a 1.2 km-thick low velocity upper layer with P- and S-wave velocities of 2.0 km/sec and 0.6 km/sec respectively. This low velocity layer is based on borehole data from the Roer Valley Graben (Budny 1984) depicting an upper sedimentary layer with a thickness varying from 1.2 to 1.4 km.

Secondly, the obtained master event locations were fixed and the station delays were obtained for all mobile and permanent stations with respect to the regional model (NL001 or model C in Ahorner & Pelzing 1983).

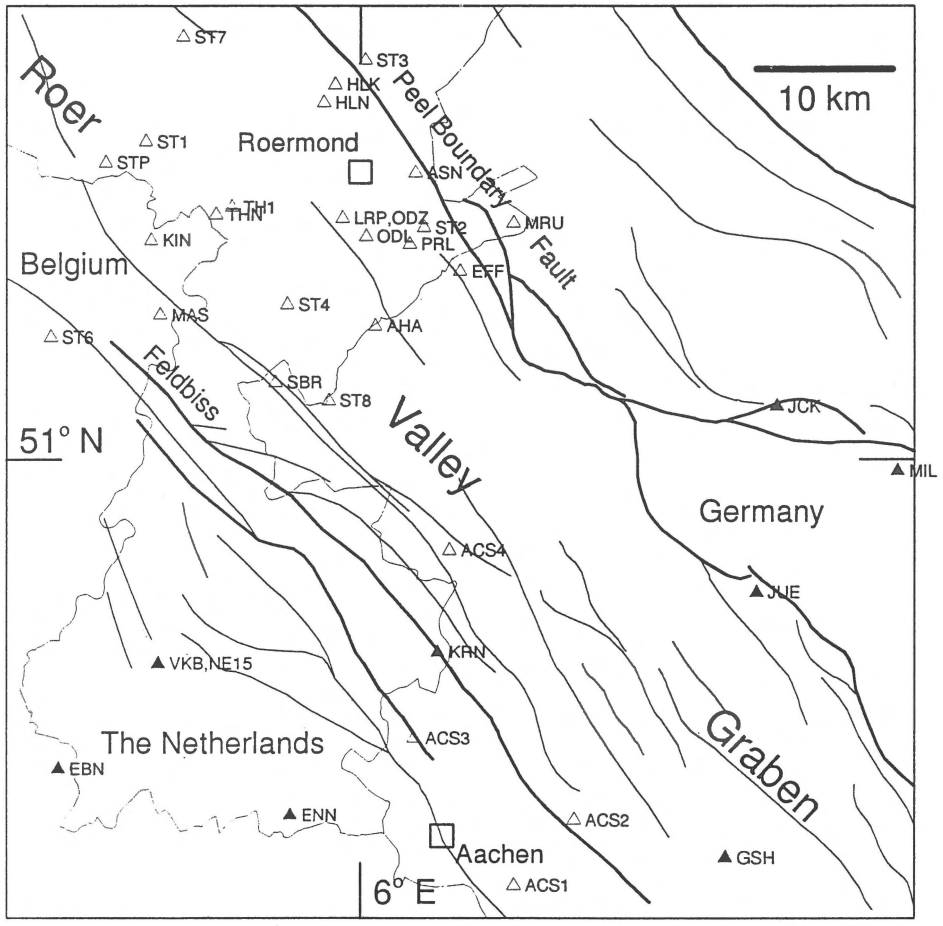

Fig. 1. Roer Valley Graben: seismic stations and tectonic framework. Mobile and permanent seismograph stations in the epicentral region are shown as △ and ▲, respectively. Faults as they appear at the surface are indicated with thick (main faults) and somewhat thinner solid lines (minor faults). Broken lines indicate international borders.

Finally, for 48 events with sufficient arrival times and a good azimuthal coverage of the recording stations, the locations were estimated using the station delays obtained in step two and velocity model NL001 that does not include a low-velocity upper layer (Table 4). For eight aftershocks that were located outside the epicentral area insufficient data inhibited the estimation of reliable station delay times (Table 4). Consequently, these events were located using model NL001 without station delays.

The aftershock and the main shock locations are shown in Fig. 4, together with the major faults as they emerge at the surface (P. van Rooijen & A. Prüffert, pers. comm.). No error bars have been depicted in the figure. However, assuming that our velocity model is correct the epicentral location errors for the 48 aftershocks in the vicinity of the main shock hypocenter average 0.9 km and the depth errors 1.0 km.

The first prominent feature that emerges from the epicentral location map is, apart from a cluster of aftershocks near the main shock epicenter, a large number of aftershock epicentra situated up to 40 km southeast of the main shock epicenter, but within the graben (Figs 4, 6). These events do have a larger epicenter location error, probably in the order of 2 km. Still, considering the uncertainties, post seismic stress field changes at such distances become insignificant as compared to regular stress changes due to earth tides (Hill et al., 1993). In this context it may be of interest to note that one aftershock at about 40 km distance from the main shock epicenter occurred three hours after the main shock (Table 2, Fig. 6).

Table 3. Mobile seismograph stations employed during the Roermond earthquake aftershock series.

Name site	Stat. code	Lat. N°	Long. E°	h m	Seismometer type	Recorder system	Agency
Haelen (NL)	HLK	51 14.88	5 58.06	30	LE-3D	Lennartz PCM	ORB (B)
Lerop (NL)	ODZ	51 09.60	5 58.56	30	LE-3D	Lennartz PCM	ORB (B)
St. Odilienberg (NL)	ODL	51 08.88	6 00.06	30	LE-3D	Lennartz PCM	ORB (B)
Stramproy (NL)	STP	51 11.74	5 43.54	30	LE-3D	Lennartz PCM	ORB (B)
Maaseik (B)	MAS	51 05.74	5 47.11	30	LE-3D	Lennartz PCM	ORB (B)
Thorn (NL)	TH1	51 10.03	5 51.62	30	LE-3D	Lennartz PCM	ORB (B)
Kinrooi (B)	KIN	51 08.68	5 46.53	30	LE-3D	Lennartz PCM	ORB (B)
Thorn (NL)	THN	51 09.70	5 50.56	30	LE-3D	Lennartz PCM	ORB (B)
Haelen (NL)	HLN	51 14.18	5 57.38	30	LE-3D	Lennartz PCM	ORB (B)
Humain (B)	HU1	50 11.21	5 13.59	290	LE-3D	Lennartz PCM	ORB (B)
Assenray (NL)	ASN	51 11.42	6 03.16	30	WMKV	Portacorder	KNMI(NL)
Lerop (NL)	LRP	51 09.62	5 58.58	30	WMKV	Portacorder	KNMI(NL)
MERU stichting (NL)	MRU	51 09.41	6 09.37	30	LE-3D	Lennartz	KNMI(NL)
Paarlo (NL)	PRL	51 08.57	6 02.80	30	LE-3D	Lennartz	KNMI(NL)
Effen (G)	EFF	51 07.50	6 06.00	30	LE-3D	Lennartz	KNMI(NL)
Schalbruch(G)	SBR	51 03.11	5 54.35	35	LE-3D	LennartzPCM	Un.C(G)
Althaaren (G)	AHA	51 05.35	6 00.65	43	LE-3D	LennartzPCM	Un.C(G)
Schleckheim (G)	ACS1	50 43.24	6 09.39		L4C	LennartzPCM	Un.A(G)
Stolberg (G)	ACS2	50 45.84	6 13.11		L4C	LennartzPCM	Un.A(G)
Richterich (G)	ACS3	50 49.07	6 03.09		L4C	LennartzPCM	Un.A(G)
Ubach-Palenburg(G)	ACS4	50 56.49	6 05.33		L4C	LennartzPCM	Un.A(G)
Tungelroij (NL)	ST1	51 12.59	5 46.15	30	L22	Telemetry	EOPG(F)
St. Ludwig (NL)	ST2	51 09.26	6 03.74	30	L22	Telemetry	EOPG(F)
Beesel (NL)	ST3	51 15.84	6 00.00	30	L22	Telemetry	EOPG(F)
Hingen (NL)	ST4	51 06.19	5 55.06	30	L22	Telemetry	EOPG(F)
Veldhoven, Limb (NL)	ST5	51 11.40	5 35.83	30	L22	Telemetry	EOPG(F)
Opoeteren (NL)	ST6	51 04.84	5 40.13	30	L22	Telemetry	EOPG(F)
Budschop (NL)	ST7	51 16.77	5 48.47	30	L22	Telemetry	EOPG(F)
Koningsbosch (NL)	ST8	51 02.41	5 57.74	30	L22	Telemetry	EOPG(F)

Aftershock hypocentra depicted in a cross section perpendicular to the main shock rupture plane with a strike of 127° coincide well with a fault plane dip of approximately 70° (Fig. 5). A rupture fault plane with strike 127° fits better with the aftershock distribution than a fault plane with a strike of 143°. In the hypocentral region only five events were estimated to be deeper than the hypocenter or rupture initiation point of the main shock at around 17.4 km (Fig. 5). This may fit well with the hypothesis that the rupture initiation point is situated close to the deepest part of the seismogenic zone within the crust.

The epicentral location of both the main shock and its nearby aftershocks suggest that they occur on the Peel Boundary Fault, assuming a straight extrapolation from its surface trace and known depth continuation down to 4 km. However, the fault plane azimuth of the main shock as obtained from our first motion solution (Fig. 7) and corroborated by Ahorner (1992, 1994), Pelzing (1994) and body wave analysis (Paulssen et al. 1992), as well as the locations of aftershocks in the vicinity of the main shock hypocenter, show an azimuth difference of about 20° with the general strike of the Peel Boundary Fault. This suggests a more complicated fault structure at 15 to 20 km depth than the one depicted by a flat plane depth extrapolation of this fault. Only the focal mechanisms of Dziewonski et al. (1993) show a strike that coincides with the strike of the Peel Boundary Fault. An unequivocal relation

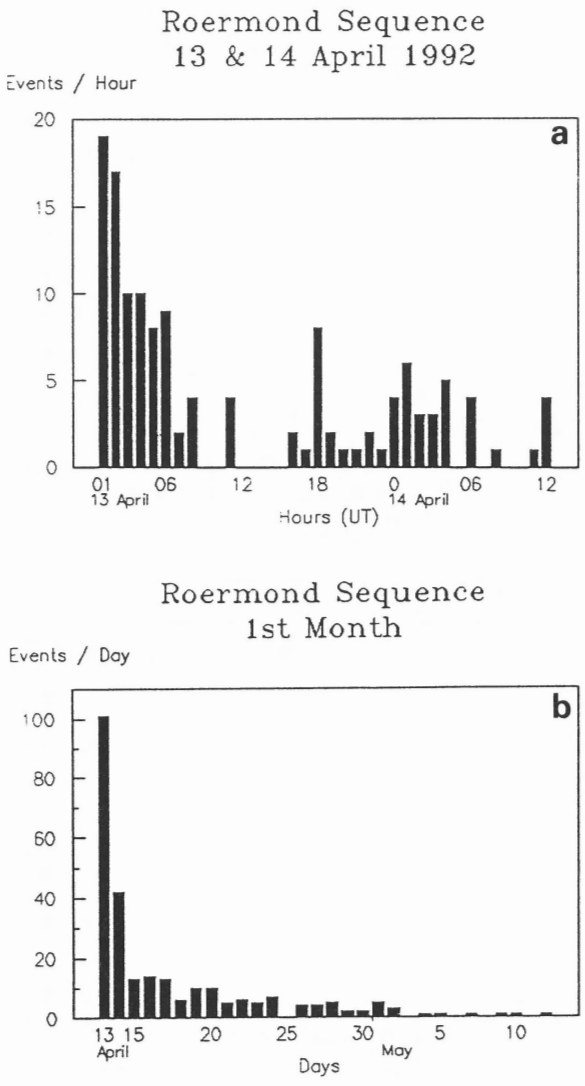

Fig. 2. Roermond aftershock occurrence. Number of aftershocks given as a function of time, a) for the first 36 hours, b) for the first month.

between the aftershocks southeast of the epicentral area and surface fault traces cannot be established.

Local magnitude determination

The event magnitudes in Table 4 have been determined from the peak ground displacement as recovered from digital seismograms of the permanent Belgian seismograph stations. The local magnitude is defined as:

$$M_L = \log A\,(\Delta) - \log A_0(\Delta)$$

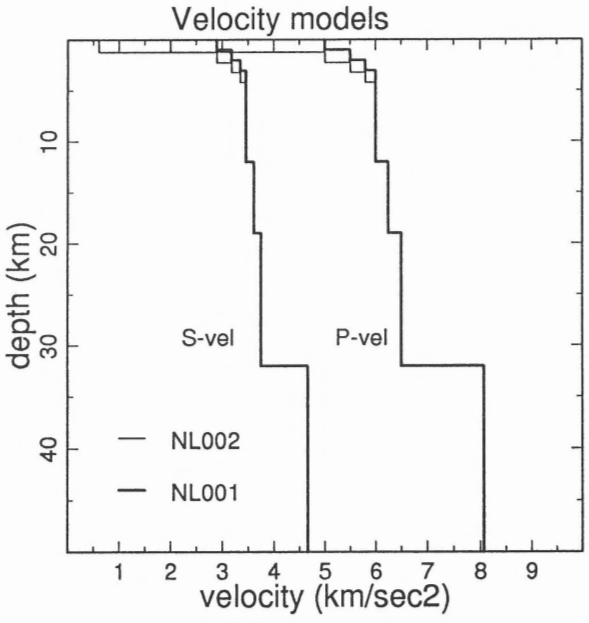

Fig. 3. Crustal velocity models. Velocity models used in locating the aftershocks (NL001, thick solid line) and the master events (NL002, deviates from NL001 in the upper 5 km and is indicated with a thin solid line).

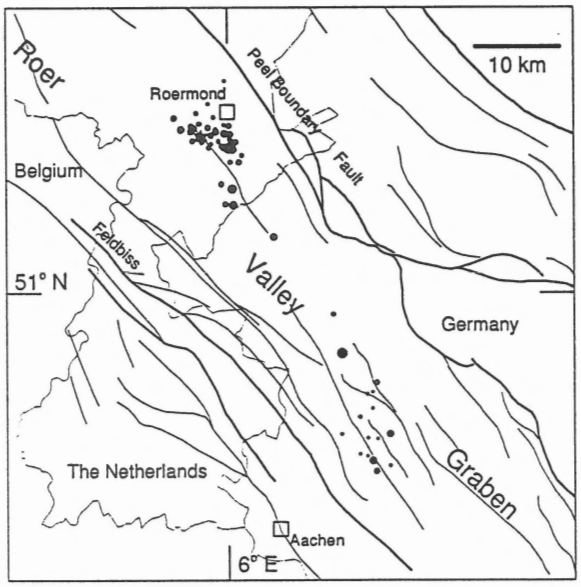

Fig. 4. Epicentral locations (Table 4) of the Roermond earthquake (solid star) and its aftershocks (solid circles). Faults are indicated as in Fig. 1. Aftershocks with $M_L \geq 1.0$ and located by Pelzing (1994) are added to the events of Table 4.

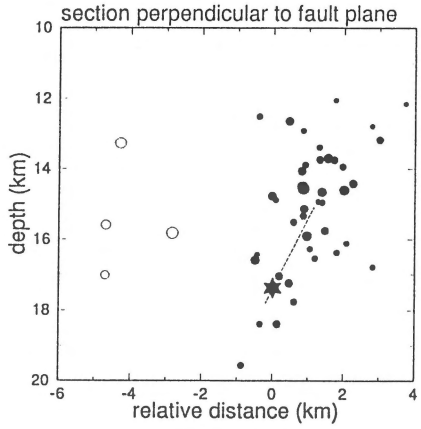

Fig. 5 a. Location of Roermond earthquake aftershocks: Event hypocentral locations projected on a plane perpendicular to the strike of the fault plane of the main shock (124°). Solid circles, aftershocks near the main shock hypocenter. Open circles, aftershocks at > 6 km distance from the main shock epicenter (see Fig. 4).

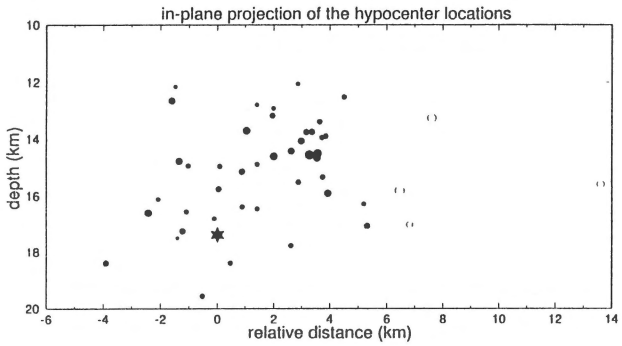

Fig. 5 b. Location of Roermond earthquake aftershocks: Event hypocentral locations projected on a vertical plane parallel to the strike of the fault plane of the main shock (124°). Solid circles, aftershocks near the main shock hypocenter. Open circles, aftershocks at > 6 km distance from the main shock epicenter (see Fig. 4). Otherwise legend as in Fig. 5a.

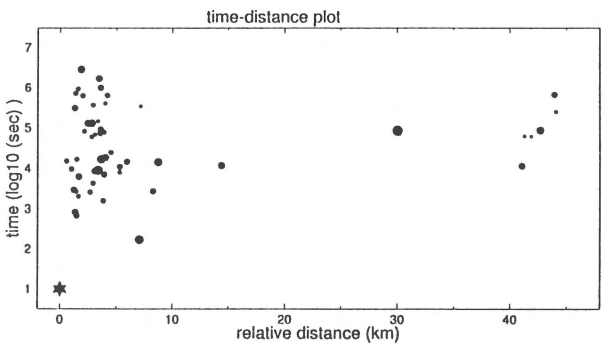

Fig. 6. Event time-distance plot for the Roermond earthquake main shock (star) and aftershocks (solid circles). The absolute distances between the main shock and the aftershock epicenters are plotted as a function of (log) time. In this Fig., aftershocks with $M_L \geq 1.0$ and located by Pelzing (1994) are added to the events of Table 4. Otherwise legend as in Fig. 5a.

where $A(\Delta)$ is the maximum ground displacement amplitude in μm at a distance Δ from the source. $A_0(\Delta)$ is the reference curve for the maximum amplitude attenuation with hypocentral distance Δ (Camelbeeck 1993).

The amplitude data for the earthquakes near Roermond are combined with the amplitude data for events recorded by the Belgian seismograph network since 1985. The combined data are inverted in order to obtain simultaneously for each earthquake a reference attenuation curve, the station correction and the magnitude. The inversion scheme used is similar to that of Alsaker et al. (1991). We used the same scaling condition for the reference attenuation curve at a distance of 17 km. At this distance the magnitudes measured from the maximum ground displacement for earthquakes in the studied area correspond to those of Californian earthquake magnitudes. The local magnitudes as determined in the present paper (Table 4) agree well with the local magnitudes of the aftershocks given by Ahorner (1994).

Fault plane solutions

For 20 aftershocks, indicated in Table 4, and the main shock we obtained the focal mechanisms. The solutions were calculated using P-wave first motion sense and a modified version of the method presented by Dillinger et al. (1972). The focal mechanisms are maximum likelihood solutions found by a grid search procedure of a likelihood function L over the 3-dimensional space (ϕ, δ, λ), where ϕ is the strike, δ the dip and λ the rake of possible fault plane.

Table 4. Located main shock and aftershocks.

#	Date y m d	O.T. h:m:s	Lat. N ° '	Long. E ° '	Depth km	M_L	# Stat.	Comments
1	920413	01:20:02.8	51 09.81	5 57.24	17.4	5.8	47	
2	920413	01:22:52.1	51 06.58	6 00.18	15.8	3.2	11	
3	920413	01:31:08.0	51 10.45	5 57.72	15.8	2.2	13	
4	920413	01:33:32.4	51 10.21	5 56.01	14.8	2.5	23	
5	920413	01:46:03.4	51 09.05	6 00.04	15.3	2.0	19	2)
6	920413	01:53:30.7	51 10.69	5 56.87	14.9	1.7	14	
7	920413	02:02:24.2	51 09.28	5 59.12	17.8	2.0	19	
8	920413	02:04:30.6	51 09.41	5 58.02	14.9	1.8	15	
9	920413	02:05:07.4	51 05.64	5 59.52	17.0	2.3	19	2)
10	920413	02:08:20.8	51 09.93	5 58.03	15.2	2.4	26	2) 3)
11	920413	02:30:41.0	51 09.19	5 59.30	15.5	2.0	21	
12	920413	03:03:26.5	51 10.50	5 56.06	12.7	2.5	26	2)
13	920413	03:17:49.7	51 11.06	5 54.27	18.4	2.3	23	2)
14	920413	03:33:45.8	51 08.69	6 01.16	16.3	1.7	12	
15	920413	03:41:27.2	51 09.26	5 59.48	14.1	2.5	24	
16	920413	03:49:42.3	51 09.19	5 59.71	14.6	3.4	30	2) 3)
17	920413	04:00:07.1	51 09.58	5 56.18	19.6	2.0	11	
18	920413	04:22:43.5	51 08.27	6 00.82	17.1	2.3	18	
19	920413	04:32:47.8	50 51.15	6 15.89	14.1	2.5	22	4)
20	920413	04:37:46.0	51 03.57	6 04.32	15.6	2.6	17	2)
21	920413	05:20:45.6	51 05.58	6 00.28	13.3	3.0	26	2)
22	920413	05:25:30.5	51 06.90	5 59.12	27.6	2.3	13	
23	920413	05:35:19.7	51 09.51	5 57.14	18.4	1.9	12	
24	920413	06:01:28.8	51 09.18	5 57.77	16.5	1.8	11	
25	920413	06:02:11.5	51 09.09	5 59.90	14.5	3.2	31	2) 3)
26	920413	06:16:35.2	51 09.34	6 00.15	14.7	2.7	22	2) 3)
27	920413	06:22:56.9	51 09.04	6 00.14	13.9	2.0	12	
28	920413	06:33:40.1	51 09.04	6 00.22	15.9	2.7	22	2) 3)
29	920413	08:18:36.9	51 08.26	5 59.59	12.5	1.9	16	
30	920413	18:01:26.9	51 11.10	5 58.27	16.8	1.7	14	
31	920413	18:34:39.6	50 49.79	6 13.60	14.8	1.1	10	4)
32	920413	18:46:23.5	50 49.93	6 12.91	13.2	1.2	6	4)
33	920413	20:19:33.2	51 10.62	5 59.33	12.8	1.5	9	
34	920413	21:50:02.4	51 10.55	5 59.82	13.2	2.2	27	2)
35	920413	22:59:21.8	51 09.28	6 00.18	13.4	2.0	21	2) 3)
36	920414	00:01:30.7	50 09.58	5 58.80	12.9	1.7	16	4)
37	920414	01:06:46.1	50 56.28	6 11.16	19.2	3.7	29	4)
38	920414	01:36:23.4	50 49.72	6 14.12	15.1	2.8	36	
39	920414	02:31:07.0	51 09.61	6 00.05	13.8	2.3	34	2) 3)
40	920414	12:41:39.5	51 10.33	5 55.02	16.6	2.7	30	2)
41	920414	12:56:32.1	51 10.09	5 59.37	14.6	2.9	33	2) 3)
42	920414	17:33:40.8	51 09.72	5 59.86	12.1	1.5	9	

Continued next page.

Table 4. continued.

#	Date y m d	O.T. h:m:s	Lat. N ° '	Long. E ° '	Depth km	M_L	# Stat.	Comments
43	920415	22:05:38.7	50 49.23	6 15.87	16.2	1.4	14	
44	920416	14:07:16.2	51 10.39	5 56.33	17.3	2.3	29	4)
45	920416	23:29:48.2	51 13.37	5 59.40	17.5	1.2	9	
46	920417	05:27:42.9	51 11.37	5 56.51	16.1	1.7	19	
47	920417	15:57:03.6	51 11.92	5 57.74	12.2	1.4	15	
48	920420	04:41:03.2	51 10.34	5 58.49	16.4	1.9	25	2) 3)
49	920420	07:27:01.5	51 09.55	6 00.56	14.0	2.0	28	2) 3)
50	920420	16:50:08.5	50 51.52	6 13.13	18.4	2.2	22	4)
51	920420	19:52:04.6	50 49.58	7 00.50	08.0	2.1 1)	20	4)
52	920421	07:52:20.2	51 10.40	5 57.71	15.0	1.9	17	
53	920423	16:19:40.3	51 10.67	5 56.78	16.6	1.8	8	
54	920424	10:35:27.2	51 09.37	5 59.99	13.8	2.3	34	2) 3)
55	920502	08:50:02.6	51 10.01	5 59.93	14.4	2.5	32	2) 3)
56	920515	19:33:26.9	51 10.18	5 58.47	13.7	2.8	23	

Notes: 1) magnitude from Ahorner (1992); 2) focal mechanism presented in Figs 7 and 8; 3) focal mechanism used in the stress inversion as described in the text; 4) events located without station delays.

Let X_i^o denote the observed first motion at station i

$$X_i^o \equiv \begin{cases} +1 \text{for compression} \\ -1 \text{for dilatation} \end{cases}$$

Further let X_i^c $(\lambda, \phi, \delta) = \pm 1$ denote the calculated first motion at station i for the focal mechanism defined by the parameters (λ, ϕ, δ). The probability that the observed first motion at station i will correspond to the calculated first motion is defined as (Camelbeeck 1993):

$$P_i = P_i(X_i^o, (\lambda, \phi, \delta)) \equiv$$
$$\equiv \tfrac{1}{2}\left[1 + X_i^o X_i^c \operatorname{erf}\left[\frac{|F_i^P(\lambda,\phi,\delta)|}{\sigma\sqrt{2}}\right]\right]$$

where F_i^P (γ, ϕ, δ) is the calculated P-wave radiation pattern factor for the P-wave ray arriving at station i due to the earthquake with focal mechanism (λ, ϕ, δ) and erf is the cumulative density function of a normal distribution. σ is a weighting factor depending on the position error of the hypocenter-station ray on the focal sphere due to, for example, inadequacy of the crustal model.

The probability is highest for stations far from the nodal plane (large values of F_i^P) and lowest for stations close to the normal plane (small values of F_i^P). The likelihood function is:

$$L(X_i^o, (\lambda, \phi, \delta)) = \prod_{i=1}^{n} P_i$$

The quality of the solution is evaluated by comparing the 90% to 95% confidence regions for the pole positions. This method gives an objective and easy interpretation of the reliability of the solutions. A good solution is characterized by small confidence regions and a poor one by large and deformed regions.

The obtained focal mechanisms are shown in Figs 7 and 8. On each diagram of Fig. 7 are indicated, the adopted value σ (0.05), the confidence level corresponding to the plotted confidence region of the poles, and P_i associated to each dataset as a function of the calculated radiation pattern coefficient F_i^P for station i for the obtained focal mechanism solution.

Stress tensor inversion

A rough estimate of the stress field in the immediate surroundings of the main shock rupture area after the main event was estimated from the obtained aftershock focal mechanisms. For this purpose we selected well-determined solutions of 13 aftershocks that occurred within the immediate vicinity of the main shock hypocenter (Table 4). Using the so-called 'exact' method of Gephart & Forsyth (1984) and Gephart (1990) we estimated the stress field that fits our data best. The results (Fig. 9) fit well with the regional stress pattern as derived from other seismicity in the region (Ahorner 1983, Camelbeeck & van Eck 1994, Carey-Gailhardis & Mercier 1992) and suggest that the main

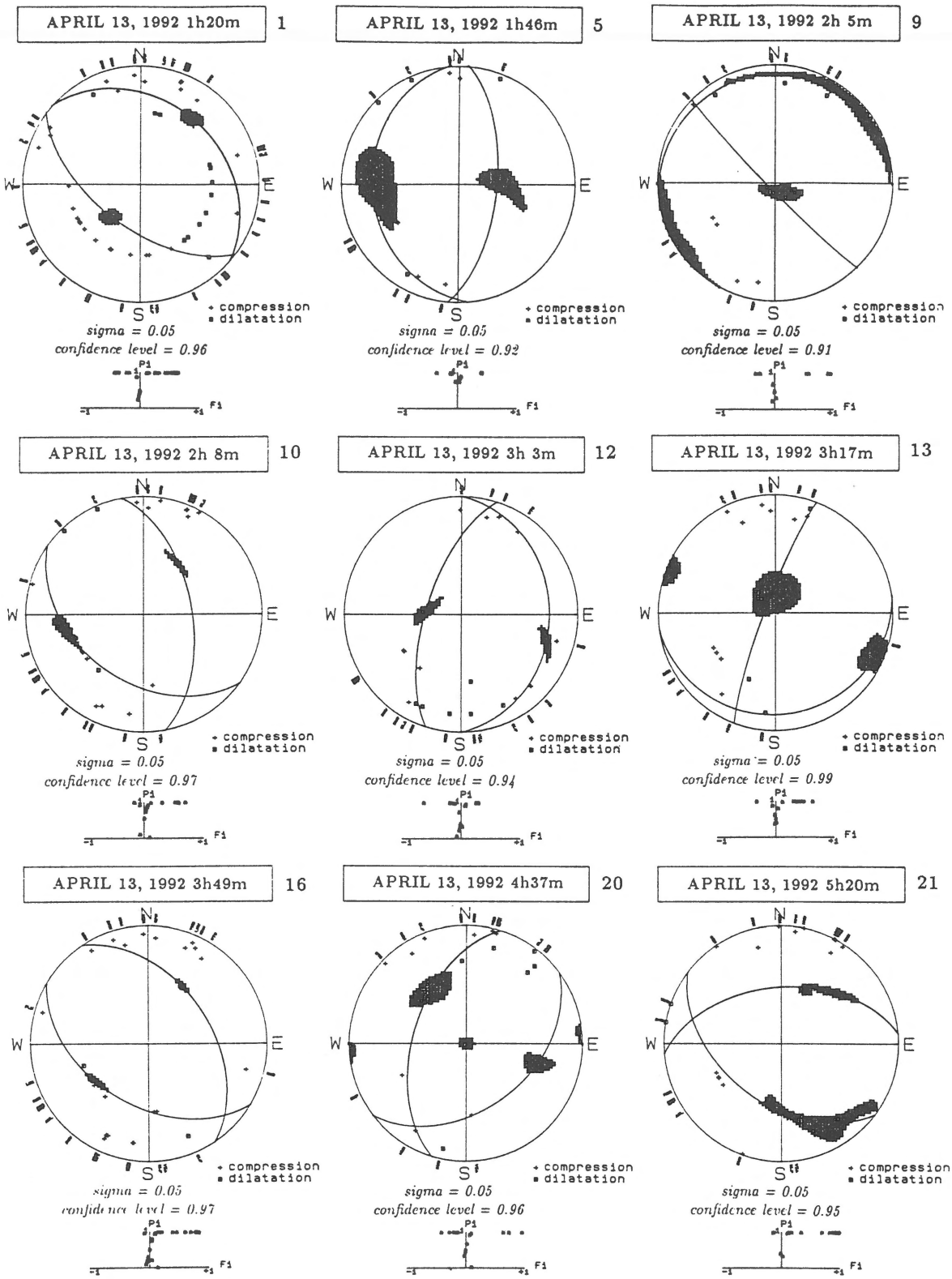

Fig. 7. Focal mechanism solutions for the 1992 Roermond earthquake and 20 aftershocks. The event numbers refer to Table 4. Pi and Fi are the probability, P_i, and radiation pattern coefficient, F_i, respectively. The two focal-plane solutions are indicated in each figure together with the dark confidence regions for the noted confidence level. Details are explained in the text. Continued next page.

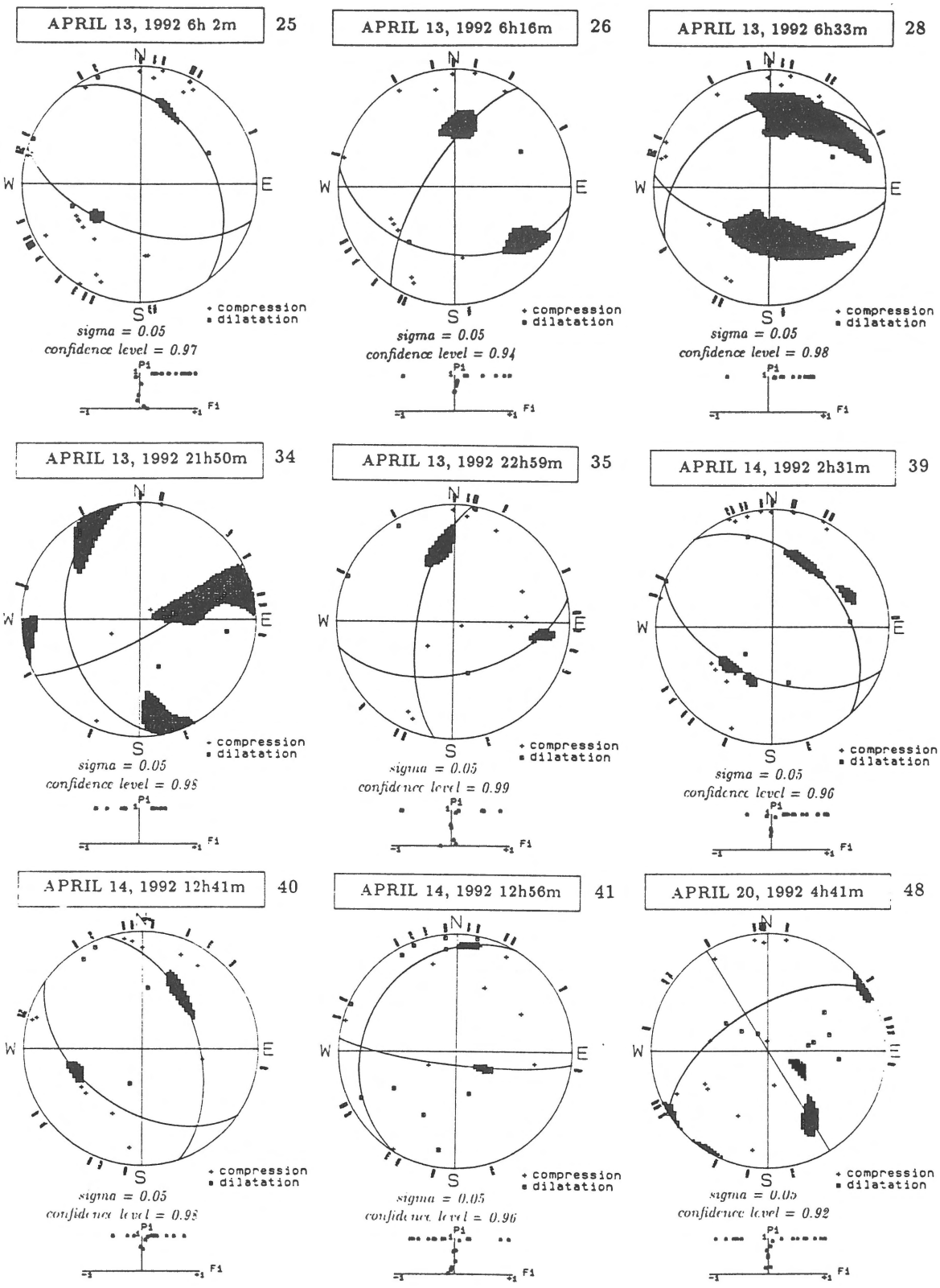

Fig. 7. Continued. Further continued next page.

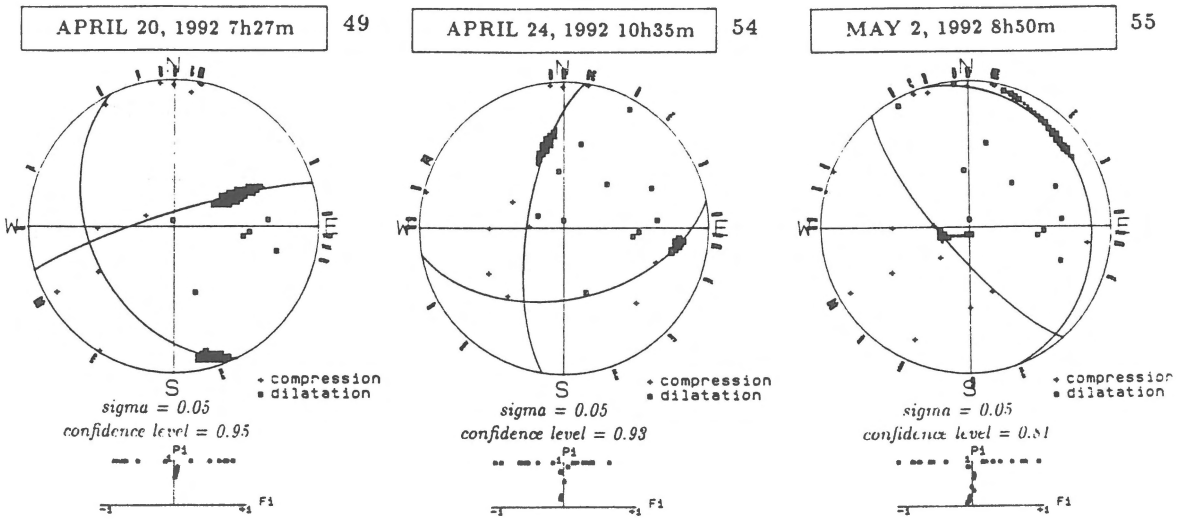

Fig. 7. Continued.

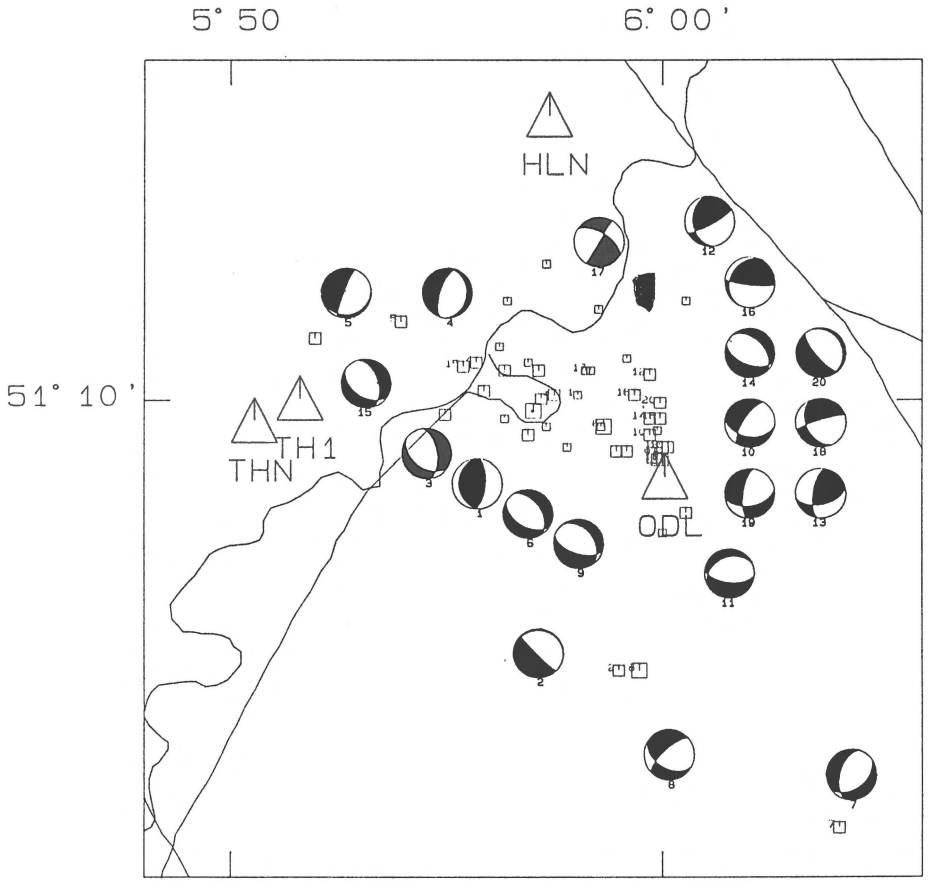

Fig. 8. Focal mechanisms for the Roermond earthquake and 20 aftershocks. Lower hemisphere focal mechanism projections with their epicentral locations. The number under each focal mechanism projection refers to its associated location (□).

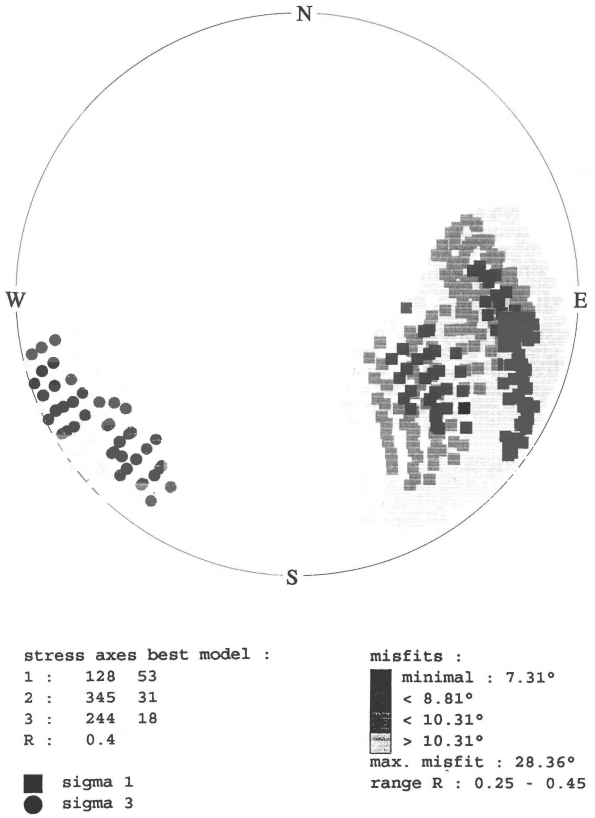

Fig. 9. Stress tensor inversion. Search for best fit of the principal stress axis to 13 aftershocks (Event numbers 10, 15, 16, 25, 26, 28, 35, 39, 41, 48, 49, 54 and 55 in Table 4). The squares (σ_1) and circles (σ_3) indicate the different test calculations. The degree of darkness indicates the misfit angle. The best (darkest) solution has a misfit angle of 7.3Δ. The maximum misfit angle considered was 28.4°. R, the stress ratio, varied between 0.25 and 0.45.

shock did not influence significantly the direction of the local stress field. However, the relative magnitude of the principal axis obviously changes, as indicated by the different kinds of focal mechanisms. Therefore, a more detailed study of the local stress field changes is warranted.

Discussion and conclusions

The Roermond earthquake had a size and location that could be expected from the present-day knowledge of seismic hazard in this region (Ahorner & Rosenhauer 1975, De Crook 1993). In northwest Europe significant onshore seismicity can be found in the Belgian zone, the Rhine Graben system and the Swabian Jura (Ambraseys 1985, Camelbeeck & van Eck 1994, Leydecker 1986, Ahorner 1970). Compared with other parts of the Rhine Graben system, the Lower Rhine Embayment, which includes the Roer Valley Graben, and the Belgian zone, show a relatively high rate of seismicity. However, on a global scale, the seismicity in northwestern Europe is low, making events with $M_W > 5$ a relatively rare phenomenon.

The normal dip-slip focal mechanism of the main shock fits well with the present-day tectonic model of the Roer Valley Graben, depicting a NE–SW tension with active rifting of the graben (Ahorner 1983, Camelbeeck & van Eck 1994, Grünthal & Stromeyer 1992). Still, intraplate pure normal dip-slip events are rare and a 70° dip for an intraplate earthquake in the lower crust should be considered remarkably steep (Jackson & White 1989).

Aftershocks occurred not only near the main shock hypocenter, but even as far as 40 km to the southeast, following the central axis of the Roer Valley Graben. Aftershocks at this relatively far distance cannot be explained by simple post-seismic stress variations caused by the main shock, as at such distance these would fall below the stress variations caused by tidal movements. No event migration with time can be found. On the contrary, one of the most distant aftershocks occurred only three hours after the main event. No aftershocks were recorded at comparable distances towards the northwest. In the hypocentral region a stress inversion of 13 aftershocks indicates that for these aftershocks the direction of the post-seismic stresses did not deviate much from those of the regional stress field model. However, even if the directions of the principal stresses are similar to the regional stress field, the relative magnitude of the principal stresses may have changed in the focal region after the main shock.

We find that little is known about the structure of the lower crust in the Roer Valley Graben (Remmelts & Duin 1990). For example, the identified rupture fault plane of the main shock suggests that a simple plane extrapolation of faults known from the uppermost crust to the lower crust is unsatisfactory. Furthermore, although the focal mechanisms of 20 aftershocks show predominantly extensional mechanisms, the fault plane strikes of the aftershocks are both parallel and perpendicular to the main fault plane. This suggests that many aftershocks do not fall on the main fault plane, but represent in many cases failure in a volume around the fault plane. Sofar we have not been able to establish any systematic pattern in the aftershock occurrence with respect to the rupture plane.

Finally, we would like to point out several practical operational aspects that need to be (re)considered according to our experience. Firstly, the aftershock sequence of more than 200 events showed a rapid decrease of activity. This makes an extremely rapid employment of aftershock monitoring equipment adamant. Under these conditions autonomous digital seismograph stations without additional requirements, such as power, telephone connections or telemetric links, are to be preferred.

Secondly, few digital seismograph stations in northwestern Europe have dynamic range large enough to record an unclipped waveform of the Roermond earthquake. Clipped seismograms are unfortunately unfit for quantitative seismic source studies. Therefore, we hope that this earthquake stimulated many agencies to install high-dynamic digital recording equipement. Rapidly falling hardware prices may facilitate the decision.

Thirdly, no acceleration measurements are available for the main event within a radius of 50 km. Considering the lack of observational acceleration data in this part of the world and the need of engineers for such observations, an investment in accelerometers within the Roer Valley Graben is worth considering. As a consequence of the Roermond earthquake seven strong motion instruments of the Syscom-type, capable to record ground accelerations up to 0.5 g, have recently been installed in the German part of the Roer Valley Graben and its vicinity by the Department of Earthquake Geology of the University of Cologne. The recording sites closest to the Roermond area are located near the Jülich and Düren area, where strong earthquakes with a comparable magnitude as that of the recent Roermond earthquake have occurred in the past.

Fourthly, digital waveform data as obtained by local networks remain still difficult to access due to the different storage media and data formatting. A cooperative effort in converting digital seismic data to a single common data format would facilitate waveform analysis. The SEED format (Dost & Sleeman 1994) may be an attractive possibility.

Acknowledgements

The KNMI thanks Lennartz Electronics for their loan of three MARS-88 mobile seismograph stations with communication logics and especially B. Haar and D. Stoll for their help with installing the system. Thanks are also due to the many people who helped in obtaining the relevant seismic data: N. Berger, B. Bukasa, C. Janssen, M. Joswig, M. Loohman-den Oudsten, H. Martin, C. Meester, K. van Gent, R. Sleeman and R. Verbeiren. Special thanks go to P. van Rooijen (Rijks Geologische Dienst, Heerlen) and A. Prüfert (Geologisches Landesamt Nordrhein-Westphalen, Krefeld) for providing the fault maps, and K. van Westen (International Training Center, Enschede) for helping digitizing these maps with ILWIS software. The mobile seismograph stations could only operate thanks to the enthousiastic help of local inhabitants.

References

Ahorner, L. 1970 Seismotectonic relations between the graben zones of the Upper and Lower Rhine Valley. In: J.H. Illies & St. Müller (eds), Graben problems. Schweitzerbant: 155–166

Ahorner, L. 1983 Historical seismicity and present-day microearthquake activity of the Rhenish Massif, Central Europe. In: K. Fuchs et al. (eds), Plateau uplift. Springer-Verlag, Berlin: 198–221

Ahorner, L. 1985 The general pattern of seismotectonic dislocations in Central Europe as the background for the Liège earthquake on November 8, 1983. In: P. Melchior (ed.), Seismic activity in Western Europe: 41–55

Ahorner, L. 1992 Das Erdbeben bei Roermond am 13 April 1992 und die daraus zu ziehenden Lehren für das Erdbebengefährdungspotential im Rheinland – Mitt. Deutsch. Geophysik. Ges. 1–2/1992: 51–57

Ahorner, L. 1994 Fault plane solutions and source parameters of the 1992 Roermond, the Netherlands, mainshock and its stronger aftershocks from regional seismic data – Geol. Mijnbouw, this issue

Ahorner, L. & R. Pelzing 1983 Seismotektonische herdparameter von digital registrierten Erdbeben der Jahre 1981 und 1982 in der westlichen Niederrheinischen Bucht – Geol. Jahrbuch 26: 35–63

Ahorner, L. & W. Rosenhauer 1975 Probability distribution of earthquake accelerations with applications to sites in the Northern Rhine area, Central Europe – J. Geophys. 41: 581–594

Alsaker, A., L.B. Kvamme, R.A. Hansen, A. Dahle & H. Bungum 1991 The M_L scale in Norway – Bull. Seism. Soc. Am. 81: 379–398

Ambraseys, N.N. 1985 Magnitude assessment of Northwestern European Earthquakes – Earthquake Eng. Struct. Dyn. 13: 307–320

Braunmiller, J., T. Dahm & K.-P. Bonjer 1994 Source mechanism of the 1992 Roermond earthquake, the Netherlands, from inversion of regional surface waves (extended abstract) – Geol. Mijnbouw, this issue

Brune, J.N. 1970 Tectonic stress and the spectra of seismic shear waves from earthquakes – J. Geophys. Res. 75: 4997–5009

Brune, J.N. 1971 Correction – J. Geophys. Res. 76: 5002

Budny, M. 1984 Seismische Bestimmung der bodendynamischen Kernwerte von Oberflachennahen Schichten in Erdbebengebieten der Niederrheinischen Bucht und ihre Ingenieursseismologische Anwendung – Ph.D. Thesis, University of Cologne, 208 pp

Camelbeeck, T. 1993 Mecanisme au foyer des tremblemens de terre et contraintes tectoniques à partir des données de réseaux

séismique locaux. Application à l'étude d'une zone intraplaque: la zone belge. Thèse de doctorat. Université Catholique Louvain. 343 pp

Camelbeeck, T. & T. van Eck 1994 The Roer Valley Graben earthquake of April 13, 1992 and its seismotectonic setting – Terra Nova 6: 291–300

Carey-Gailhardis, E. & J.L. Mercier 1992 Regional state of stress, fault kinematics and adjustments of blocks in a fractured body of rock: Application to the microseismicity of the Rhine graben – J. Struct. Geol. 14: 1007–1017

De Crook, T. 1993 Probabilistic seismic hazard assessment for The Netherlands – Geol. Mijnbouw 72: 1–13

Dillinger, W.H., S.T. Harding & A.J. Pope 1972 Determining maximum likelihood focal plane solutions – Geophys. J. Royal Astr. Soc. 30: 315–329

Dost, B. & R. Sleeman 1994 Exchange of digital seismological waveform data in Europe: Status as illustrated by data collection for the 1992 Roermond earthquake, the Netherlands – Geol. Mijnbouw, this issue

Dziewonski, A.M., G. Ekström & M. Salganik 1993 Centroid-moment tensor solutions for April-June 1992 – Phys. Earth Planet. Int. 77: 151–163

Geluk, M.C., E.J.Th. Duin, M. Dusar, R.H.B. Rijkers, M.W. van den Berg, & P. van Rooijen 1994 Stratigraphy and tectonics of the Roer Valley Graben – Geol. Mijnbouw, this issue

Gephart, J.W. 1990 FMSI: A FORTRAN program for inverting fault/slickenside and earthquake focal mechanism data to obtain the regional stress tensor – Computers and Geosciences 16: 953–989

Gephart, J.W. & D.W. Forsyth 1984 A method for determining the regional stress tensor using earthquake focal mechanism data: Application to the San Fernando earthquake sequence – J. Geophys. Res. 89: 9305–9320

Grünthal, G. & H. Grosser 1992 Roermond Erdbeben vom 13 April 1992: Zu physikalischen Herdparametern und zur makroseismischen Herdtiefenschätzung. In: Report by the Arbeitsgruppe Wisstechn. Task Force und Erdbebenkatastrophenforschung, Hannover: 2/1–2/4

Grünthal, G. & D. Stromeyer 1992 The recent crustal stress field in Central Europe: Trajectories and finite element modeling – J. Geophys. Res. 97: 11,805–11,820

Haak, H.W., J.A. van Bodegraven, R. Sleeman, R. Verbeiren, L. Ahorner, H. Meidow, G. Grünthal, P. Hoang-Trong, R.M.W. Musson, P. Henni, Z. Schenkova & R. Zimova 1994 The macroseismic map of the 1992 Roermond earthquake, the Netherlands – Geol. Mijnbouw, this issue

Hanks, T.C. & H. Kanamori 1979 A moment-magnitude scale – J. Geophys. Res. 84: 2348–2350

Hill, D.P. et al. 1993 Seismicity remotely triggered by the magnitude 7.3 Landers, California, earthquake – Science 260: 1617–1623

Jackson, J.A. & N.J. White 1989 Normal faulting in the upper continental crust: observations from regions of active extension – J. Struct. Geology 11: 15–36

Leydecker, G. 1986 Erdbebenkatalog für die Bundesrepublik Deutschland mit Randgebieten für die Jahre 1000–1981. Geologisches Jahrbuch, Reihe E, 36, 83 pp

Lienert, B.R., E. Berg & L.N. Frazer 1986 Hypocenter: An earthquake location method using centered, scaled, and adaptively damped least squares – Bull. Seismol. Soc. Am. 76: 75–311

Meidow, H. 1994 Comparison of the macroseismic field of the 1992 Roermond earthquake, the Netherlands, with those of large historical earthquakes in the Lower Rhine Embayment and its vicinity – Geol. Mijnbouw, this issue

Oncescu, M.-C., Th. Camelbeeck & H. Martin 1994 A note on the foreshock of the 1992 Roermond earthquake, the Netherlands – Geol. Mijnbouw, this issue

Paulssen, H., B. Dost & T. van Eck 1992 The April 13, 1992 earthquake of Roermond (The Netherlands); first interpretation of the NARS seismograms – Geol. Mijnbouw 71: 91–98

Pelzing, R. 1994 Source parameters of the 1992 Roermond earthquake, the Netherlands, and some of its aftershocks recorded at the stations of the Geological Survey of NorthRhine-Westphalia – Geol. Mijnbouw, this issue

Remmelts, G. & E.J.Th. Duin 1990 Results of a regional deep seismic survey in The Netherlands. In: B. Pinet & C. Bois (eds), The potential of deep seismic profiling for hydrocarbon exploration, Edition Technip, Paris 1990: 335–343

Ziegler, P.A. 1992 European Cenozoic rift system – Tectonophysics 208: 91–111

Zijerveld, L., R. Stephenson, S. Cloetingh, E. Duin & M.W. van den Berg 1992 Subsidence analysis and modelling of the Roer Valley Graben (SE Netherlands) – Tectonophysics 208: 159–171